

MICROCOPY RESOLUTION TEST CHART
NATIONAL BUREAU OF STANDARDS - 1963 - A

AFGL-TR-82-0359

3

AD A122074

GRANT NO. AFOSR-80-0001

IONOSPHERIC RESEARCH USING SATELLITES

D. Yeboah-Amankwah
and
V.C.K. Kakane

Department of Physics
University of Ghana
Legon, Ghana.

Final Scientific Report.

Approved for public release: distribution unlimited

DTIC
ELECTE
DEC 6 1982
S B D

Prepared for:

AIR FORCE OFFICE OF SCIENTIFIC RESEARCH
Arlington, Virginia, U.S.A.

EUROPEAN OFFICE OF AEROSPACE RESEARCH AND DEVELOPMENT,
LONDON, ENGLAND.

FILE COPY

02 12 06 073

REPORT DOCUMENTATION PAGE		READ INSTRUCTIONS BEFORE COMPLETING FORM	
1. Report Number AFGL-TR-82-0359	2. Govt Accession No. AD-A122074	3. Recipient's Catalog Number	
4. Title (and Subtitle) IONOSPHERIC RESEARCH USING SATELLITES		5. Type of Report & Period Covered Final Scientific Report 1 June 1980 - 31 May 1981	
		6. Performing Org. Report Number	
7. Author(s) D. YEBOAH-AMANKWAH AND V.C.K. KAKANE		8. Contract or Grant Number AFOSR - 80-0001	
9. Performing Organization Name and Address Department of Physics University of Ghana P.O. Box 63 Legon, Ghana.		10. Program Element, Project, Task Area & Work Unit Numbers 62101F 464305BP	
11. Controlling Office Name and Address Air Force Geophysics Laboratory (AFSC) Hanscom Air Force Base, Mass, 01731 Monitor/John P. Mullen/PHY		12. Report Date 1 July, 1982.	
		13. Number of Pages 25	
14. Monitoring Agency Name and Address		15. UNCLASSIFIED	

16. & 17. Distribution Statement

Approved for public release; distribution unlimited.

18. Supplementary Notes

19. Key Words Scintillation, Depth of Fade
 Equator Seasonal distribution
 Onset and cessation time Magnetic activity

20. Abstract

Equatorial scintillation on the 257MHz signals from Marisat 1 satellite during 1980 is reported. Scintillation index and depth of fade are the two parameters used in the analysis. Seasonal variation of scintillation and the correlation between scintillation and geomagnetic activity were examined. The results confirm earlier observations on the 136 MHz signals made at Legon (Koster, 1972). Except for a few differences, these results are similar to observations on 1.5 GHz made at Huancayo. Apart from May-August, scintillations are negatively correlated with geomagnetic activity in the remaining part of the annual cycle.

CONTENTS

	<u>Page</u>
LIST OF FIGURE CAPTIONS	iii
ABSTRACT	iv
FORWARD	v
INTRODUCTION	1
EQUIPMENT	2
DATA ANALYSIS	2
SEASONAL VARIATION OF DEPTH OF FADE AND SCINTILLATION INDEX	3
ONSET AND CESSATION OF SCINTILLATION	5
SCINTILLATION AND GEOMAGNETIC ACTIVITY	6
SUMMARY OF OBSERVATIONS	6
REFERENCES	8



Accession For	
NTIS GRA&I	<input checked="" type="checkbox"/>
DTIC TAB	<input type="checkbox"/>
Unannounced	<input type="checkbox"/>
Justification	
By _____	
Distribution/	
Availability Codes	
Dist	Avail and/or Special
A	

Figure Captions

1. Typical calibration curves for some selected days.
2. Hourly variation of depth of fade (DF) on 257 MHz signals averaged over the same hour of each day of the month for 17 to 7 hours local time.
3. Average daily variation of depth of fade (DF) on 257 MHz signals between 17 hours local time and 6 hours following day for (a) January-July and (b) August-December.
4. Average hourly scintillation index (S.I.) on 257 MHz signals over the same hour of each day of the month from 17 to 6 hours local time.
5. Daily scintillation index (S.I.) on the 257 MHz signals averaged over 17 to 7 hours for each month.
6. Time integrated seasonal variation of (a) depth of fade and (b) scintillation index for 1980.
7. Average of half-widths of scintillation and depth of fade on the 257 MHz signals for each month of 1980.
8. Seasonal variation of average time of (a) onset of scintillation and (b) cessation of scintillation for each month of 1980. (c) Variation of time between onset and cessation of scintillation.
9. Plot of correlation coefficient of sum k_p versus (i) integrated scintillation coefficient and (ii) integrated depth of fade for each month.

ABSTRACT

Equatorial scintillation on 257.55 MHz signals from Marisat 1, measured at Legon (5.63°N , 0.19°W , dip 8°S) in 1980, has been analysed for monthly and seasonal variation. The relation of scintillation with magnetic activity has also been examined and, except for the period May - August which shows a small positive correlation, scintillation was found to be negatively correlated with magnetic activity.

The observed seasonal behaviour of scintillation was found to be similar to early reports based on different frequencies (Koster 1972). A report of measurements on equatorial scintillations at Huancayo (12.04°S ; 75.33°W ; dip 2°N) on 1.5GHz (Basu et al, 1980) also shows similar structure except that there, scintillation seems to be restricted to post sunset and local midnight.

FORWARD

This report is based only on measurements conducted at Legon in 1980.

We wish to express our gratitude to Messrs S.K. Osei and Mr. Daniel Sallah who provided routine maintenance of equipment and to Christopher Theodore for data reduction and key punching.

Professor J.R. Koster designed and constructed the equipment used in the measurement. Our debt to his contribution is acknowledged.

EQUATORIAL SCINTILLATION ON THE 257MHz
SIGNALS FROM MARISAT SATELLITE DURING 1980

1. Introduction

Since the last report by Koster (1978), scintillation and Faraday rotation measurements using signals from a number of satellites available above the horizon at Legon (5.63°N; 0.19°W; dip 8°S) have continued to be recorded. These measurements are listed in Table 1.

Scintillation measurements on the 257.55 MHz signal from Marisat 1 which were started in 1977 (Koster 1978), have continued through to August 1981 and this report deals with the results for 1980. Attempts made to obtain scintillation data at 1500 MHz using transmissions from Marisat 1 were not successful. It is hoped that such measurements will become possible when the 30ft-dish is fully installed at Legon.

SCINTILLATION DATA

<u>Satellite</u>	<u>Frequency in MHz</u>	<u>Elevation in degrees</u>	<u>Recording Period</u>
1. Sirio	136.140	70°	Jan. 1978 - Oct. 1980 August - December 1981
2. ATS-5	136.470	11°	Jan. 1978 - June 1979
3. Marisat 1	257.550	70°	Jan. 1978 - August 1981

FARADAY ROTATION DATA

1. ATS-5	136.470	11	Jan. 1980 - May 1981
2. Sirio	136.140	70	Jan. - Nov. 1978

Table I

2. Equipment

A phase switching system based on a 30-foot paraboloid antenna was employed in the scintillation measurements. A polarimeter based on two helical antennae was used to measure Faraday rotation. The effective radiation pattern of the two antennae, equivalent to a single dipole field, was electronically rotated through various angles at intervals by introducing selected phase paths between the antennae. Both systems are described by Koster (1978).

3. Data Analysis

In this report, data on the 257.55 MHz signals from the Marisat 1 Satellite are presented. The format of the presentation is different from that of earlier reports produced at Legon. With sudden unexpected departure of our data analysts, old computer programmes were lost and new ones have had to be developed, hence the departure from the old system.

The receiver output was calibrated at regular intervals by putting in standard signal strengths measured in decibels and observing the resulting recorder readings. By the least square method, the two readings were then fitted to a straight line which was used to convert recorder readings to signal strength.

Signal strength variation of up to 15-18 db produced linear recorder readings. For higher signal strengths up to 20 db there were severe deviations from a straight line. This can be seen from the three selected calibration curves shown in Fig.1 which show typical calibration curves for some selected days. The signal strengths so obtained were used to calculate

(a) depth of fade (DF) and (b) scintillation index (S.I.) defined for each 15-minute interval as follows:-

$$DF = (P_{MX} - P_{MIN})$$
$$S.I. = \frac{P_{MX} - P_{MIN}}{P_{MX} + P_{MIN}} \times 100$$

P_{MX} = Power of the third highest peak and
 P_{MIN} = Power of the third deepest trough in the same 15-minute interval.

4. Seasonal Variation of Depth of Fade and Scintillation Index

(a) Depth of fade

In Fig.2, we have plotted the monthly average of the depth of fade for the hours between 17 hours and 7 hours (GMT) the following morning. The graph shows the following features:

- (1) Depth of fade is essentially zero during the day in the equatorial region until 19 hours.
- (2) It rises to a peak (or sometimes two) quickly before midnight and gradually decays to zero around but before local sunrise at 6 hours (GMT).
- (3) The depth of fade shows the following average features:

Maximum of 7dB in March
Minimum of 1.8dB in June
Maximum of 5.6dB in October and
Minimum of 1.1dB in November.

Fig.3(a & b) is the plot of the daily average of depth of fade for each month. The graph shows that:

- (1) The daily variation of day to day depth of fade is quite random.
- (2) The months January - March and August - October exhibit the wildest fluctuations while May - June are quietest.

(b) Scintillation

Fig.4 shows the hourly average of scintillation index over each month of the year.

- (1) Except for October (when it occurs earlier) scintillation starts around 19 hours each day.

- (2) Scintillation index is highest in the January-April period with maximum (25% average) around midnight.

Fig.6 is a plot of the time integrated:

- (1) depth of fade and (2) scintillation index versus month of the year to show seasonal variation of these quantities.

The results clearly confirm the pattern shown in earlier figures.

- (3) The depth of fade which shows a peak each in March and October was also followed by a trough each in June and December respectively. The depth of fade thus shows a semi-annual variation.

- (4) On the average, scintillation index shows a peak of 25% in March, a trough of 7% in June, followed by a minor peak of 19% in August. The variation from September to January is relatively flat remaining around 16%.

Fig.7

In this figure the widths of scintillation and depth of fade intensities for each month have been plotted. Width is here defined as the time difference in hours, between the times of half-width intensities for S.I. and DF at dusk and dawn respectively. This time approximately measures the effective time of active scintillation for the particular day. The times have been averaged over each month and they are plotted against month of year to show their seasonal variation.

- (1) As may be expected because of their common origin, the depth of fade and scintillation index show similar variation over the year.

- (2) Scintillation activity is longest during the periods January-February and October-December where the half-width is about (8 ± 1) HRS.
- (3) Scintillation lasts shortest around May and June where scintillation activity has average half-width of about (3.5 ± 0.5) hours. This, as has been pointed out, corresponds to the period of lowest average scintillation activity. On a number of nights during this period, no scintillation is observed to occur.

5. Onset and cessation of scintillation

In Fig.8 the time of onset of scintillation averaged over each month has been plotted as (a) while a similar plot for time of cessation of scintillation is shown as (b). Plot (c) shows the seasonal variation of the difference between the times of onset and cessation of scintillation for each month. It is observed that:

- (1) Scintillation activity lasts shortest in June - about two hours. It is to be pointed out that there are a few nights during June when no scintillation is observed at all. For the particular period under consideration, namely January - December, 1980, only 18 of the 30 days of June, 1980 showed any scintillation at all.
- (2) The months January-March and September-November show the longest periods of scintillation activity. There are approximately (7.0 ± 1) hours of activity each day. Scintillation usually starts at (20.5 ± 0.5) hours and usually ends around (4.5 ± 0.5) hours following morning. The corresponding sunset and sunrise times

350 km are 19.2 and 4.8 hours respectively.

6. Scintillation and magnetic activity

Fig. 9 shows a plot of correlation coefficient between the sum kp index for the day of the record and the (i) integrated scintillation index on one hand and (ii) integrated depth of fade for each day on the other.

The variation of the correlation coefficient is quite random, however, the plot indicates that the coefficient is negative more often than it is positive. This suggests that disturbed days are more likely to show less scintillation effects than the non disturbed days. The data base is small and more statistical data would be required to establish this more firmly.

7. Summary of observations

(a) Diurnal variation of scintillation

- (i) Scintillation at the 257 MHz was observed to occur essentially during night-time - starting after sunset and ending before sunrise at 350 km. The exact times for start and cessation depends on the time of year.
- (ii) Scintillation, as reflected by S.I. and DF, quickly builds up in intensity reaching a maximum around (22.0 ± 1.0) hours. Subsequently it decays gradually to zero before sunrise at 350 km. On a few occasions, a second scintillation peak intensity smaller than the first was observed to occur after midnight.

(b) Seasonal variation

- (i) Scintillation shows equinoctial maxima in March and October and a minimum in June, near the winter solstice (Fig.6). The level

of the peak scintillation intensity in March is higher than the October maximum (Fig.7).

- (ii) The onset and cessation of scintillation depend on the time of year although scintillation always appears to start after sunset and ends before sunrise. Scintillation is earliest in March and September but is delayed in May-June (see Fig.8). Correspondingly, cessation of scintillation is delayed longest in January-March and September-November but is earliest in May-July.
- (iii) Average duration time of scintillation is longest in January-March and September-November when it may last for (7.0 ± 0.5) hours and shortest in June when it lasts on the average (2.2 ± 0.2) hours. There are indeed days during this period when scintillation may not occur at all throughout the night.

(c) Magnetic activity and scintillation

- (i) The limited data suggest that outside of the period May-August, scintillation index is negatively correlated with sun magnetic activity (Fig.9); high magnetic activity would indicate low scintillation activity.

References

1. Basu, Sunada Basu, Santimay and Mullen, J.P.

Long-term 1.5 GHz amplitude scintillation measurements at the magnetic equator. Geophysical Research Letters Vol.7 No.4 pp.259-262 (1980).

2. Koster, J.R. Equatorial Scintillation Planet Space Sci.

(1972) Vol.20 pp.1999-2014.

3. Koster, J.R. Phase and amplitude scintillation at the equator.

Department of Physics, University of Ghana, Legon, Accra (1978).

Title of Figures

1. Typical calibration curves for some selected days.
2. Hourly variation of depth of fade (DF) on 257 MHz signals averaged over the same hour of each day of the month for 17 to 7 hours local time.
3. Average daily variation of depth of fade (DF) on 257 MHz signals between 17 hours local time and 6 hours following day for (a) January-July and (b) August-December.
4. Average hourly scintillation index (S.I.) on 257 MHz signals over the same hour of each day of the month from 17 to 6 hours local time.
5. Daily scintillation index (S.I.) on the 257 MHz signals averaged over 17 to 7 hours for each month.
6. Time integrated seasonal variation of (a) depth of fade and (b) scintillation index for 1980.
7. Average of half-widths of scintillation and depth of fade on the 257 MHz signals for each month of 1980.
8. Seasonal variation of average time of (a) onset of scintillation and (b) cessation of scintillation for each month of 1980. (c) Variation of time between onset and cessation of scintillation.
9. Plot of correlation coefficient of sum k_p versus (i) integrated scintillation coefficient and (ii) integrated depth of fade for each month.

Fig 1

•••

CALIBRATION PLOTS FOR SELECTED DAYS

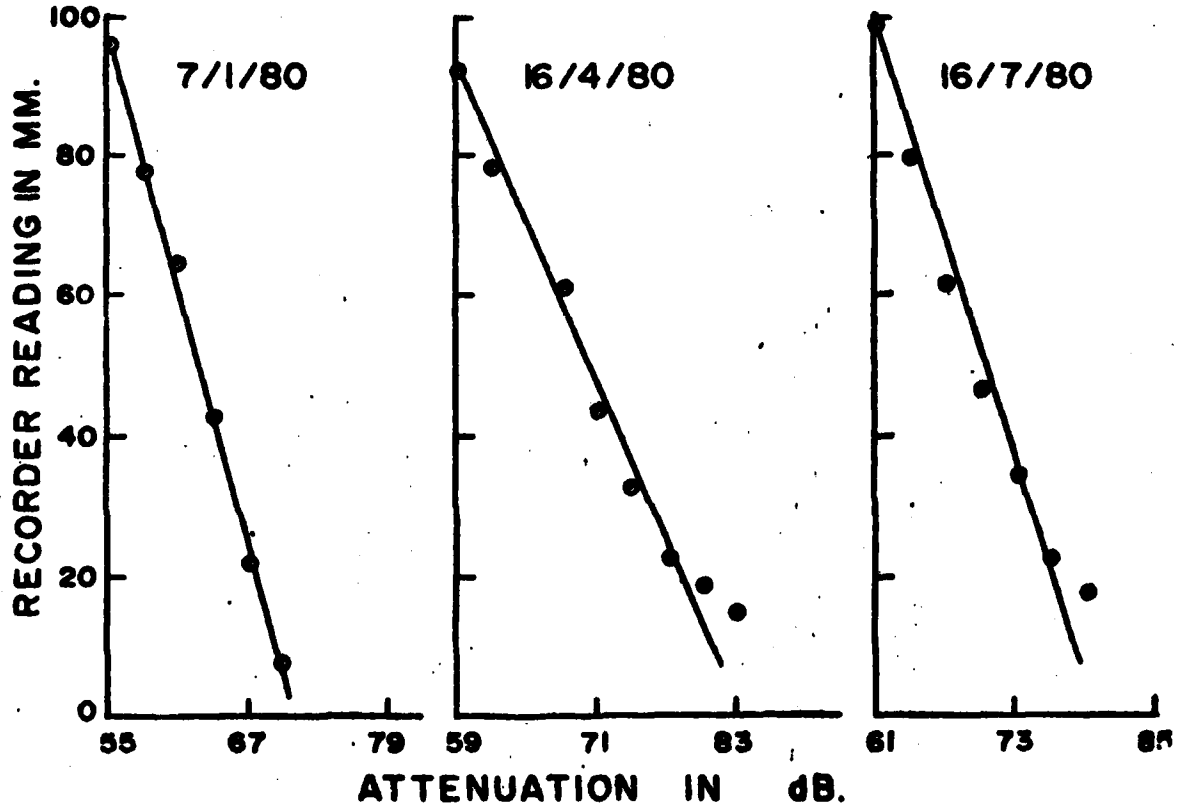


Figure 1

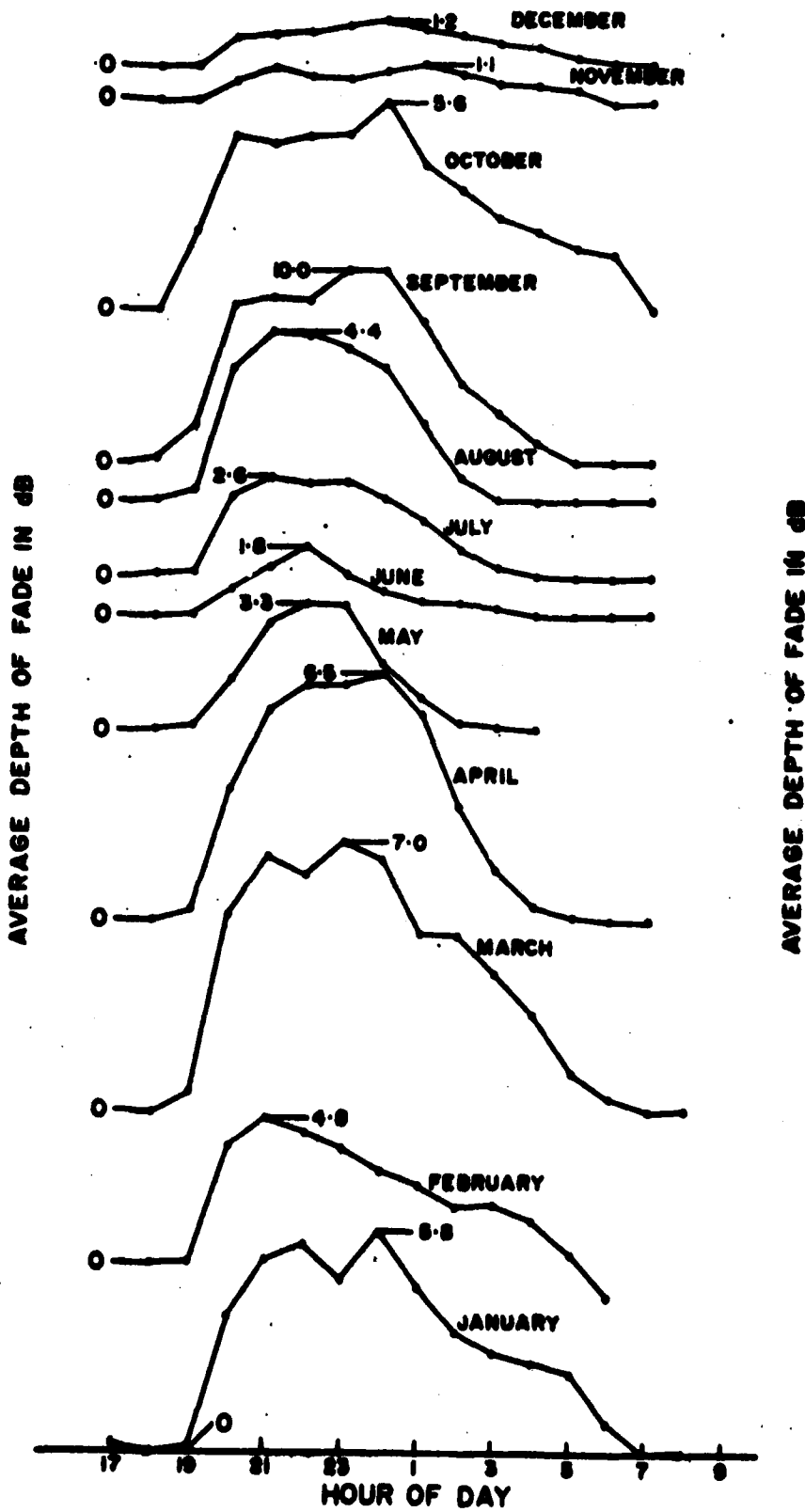


Figure 2

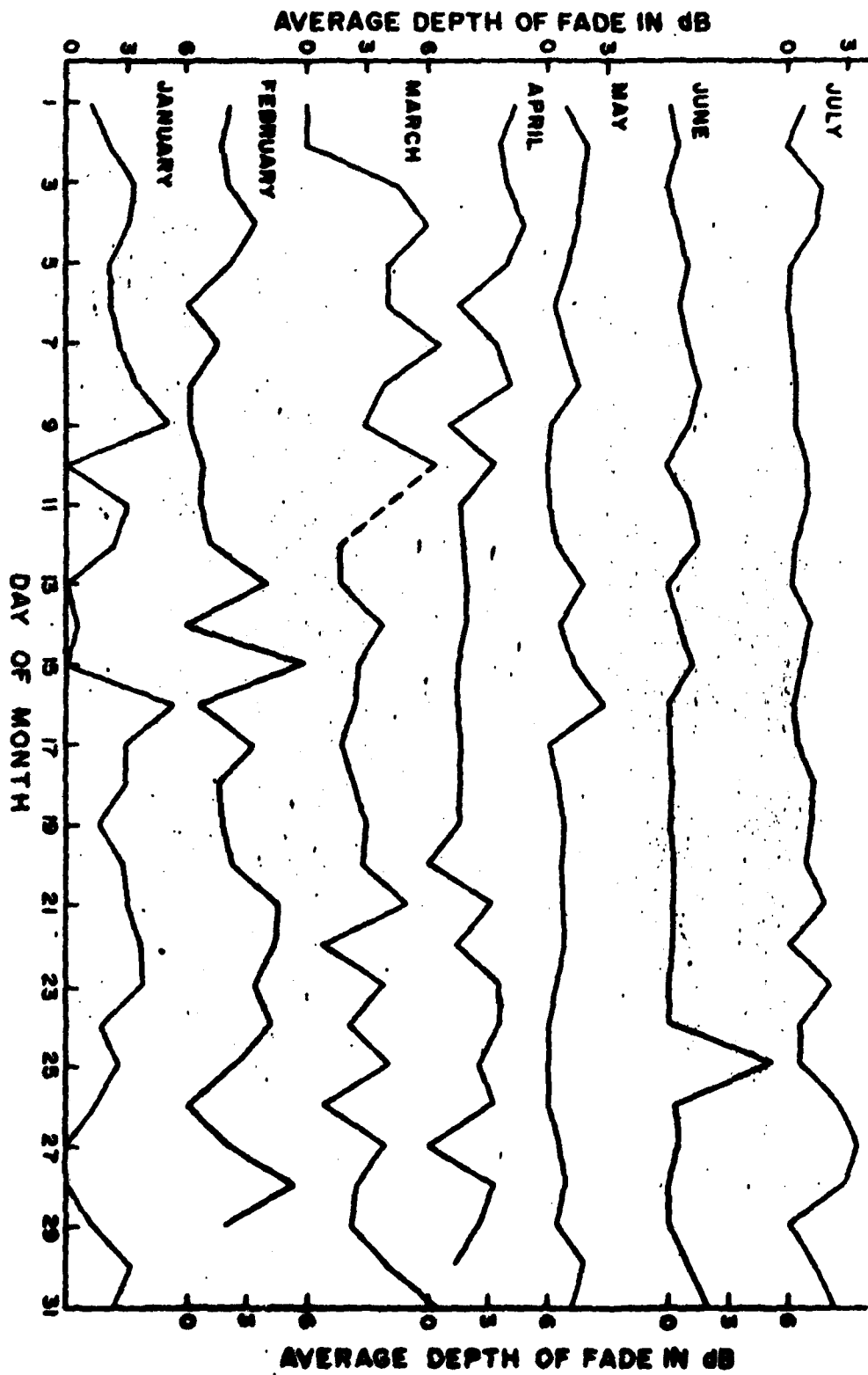


Figure 3a

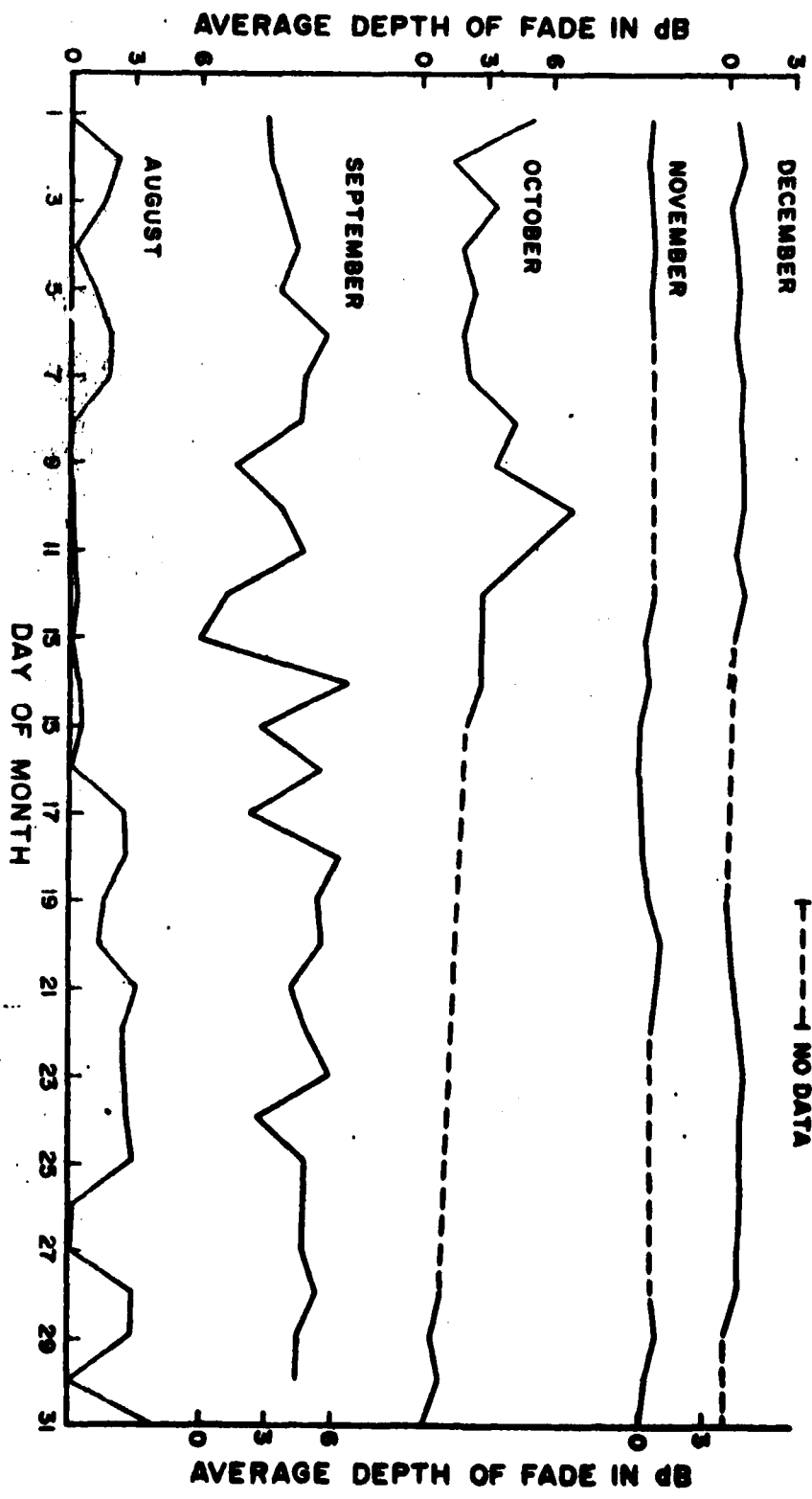


Figure 20

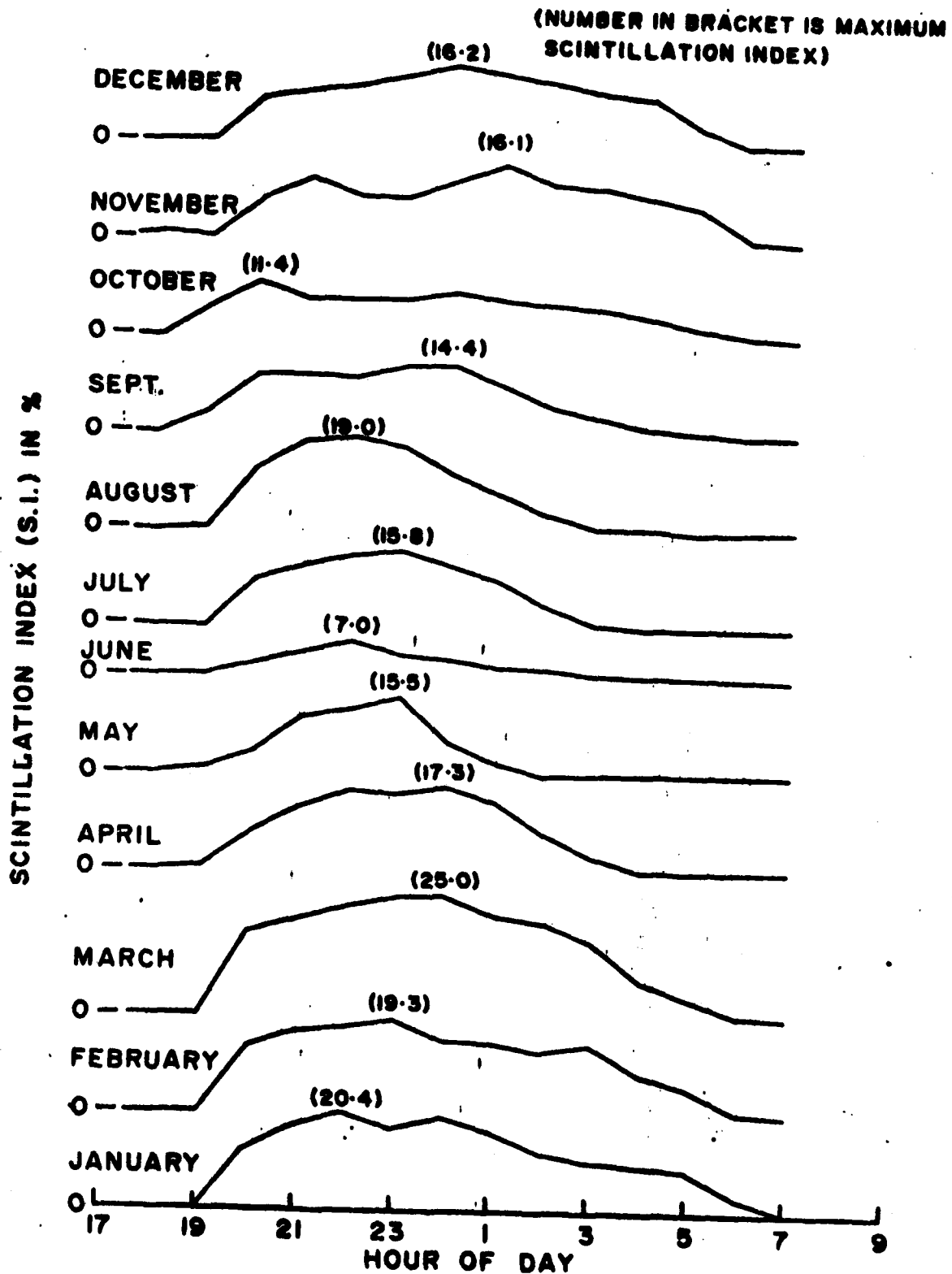


Figure 4

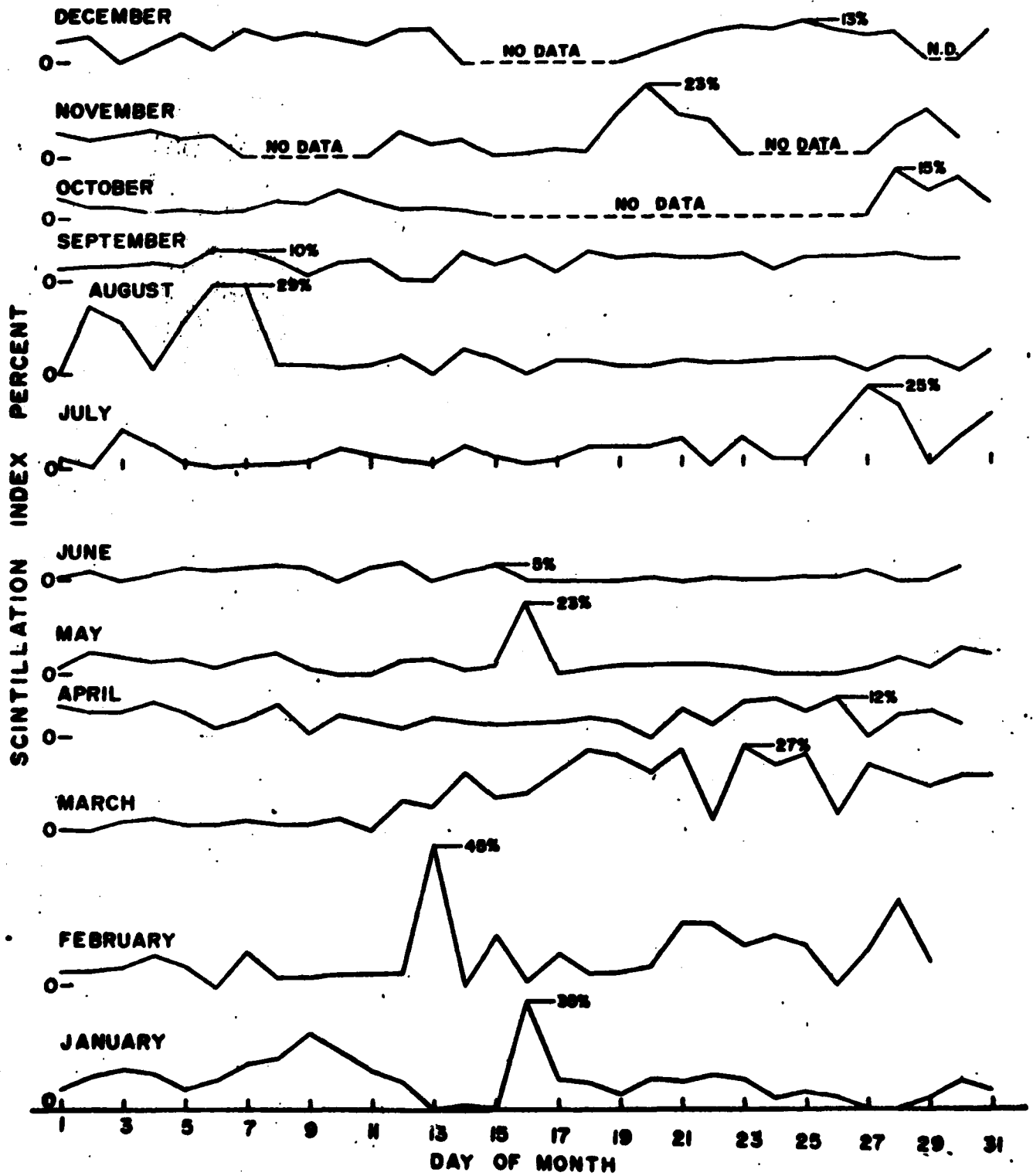


Figure 5

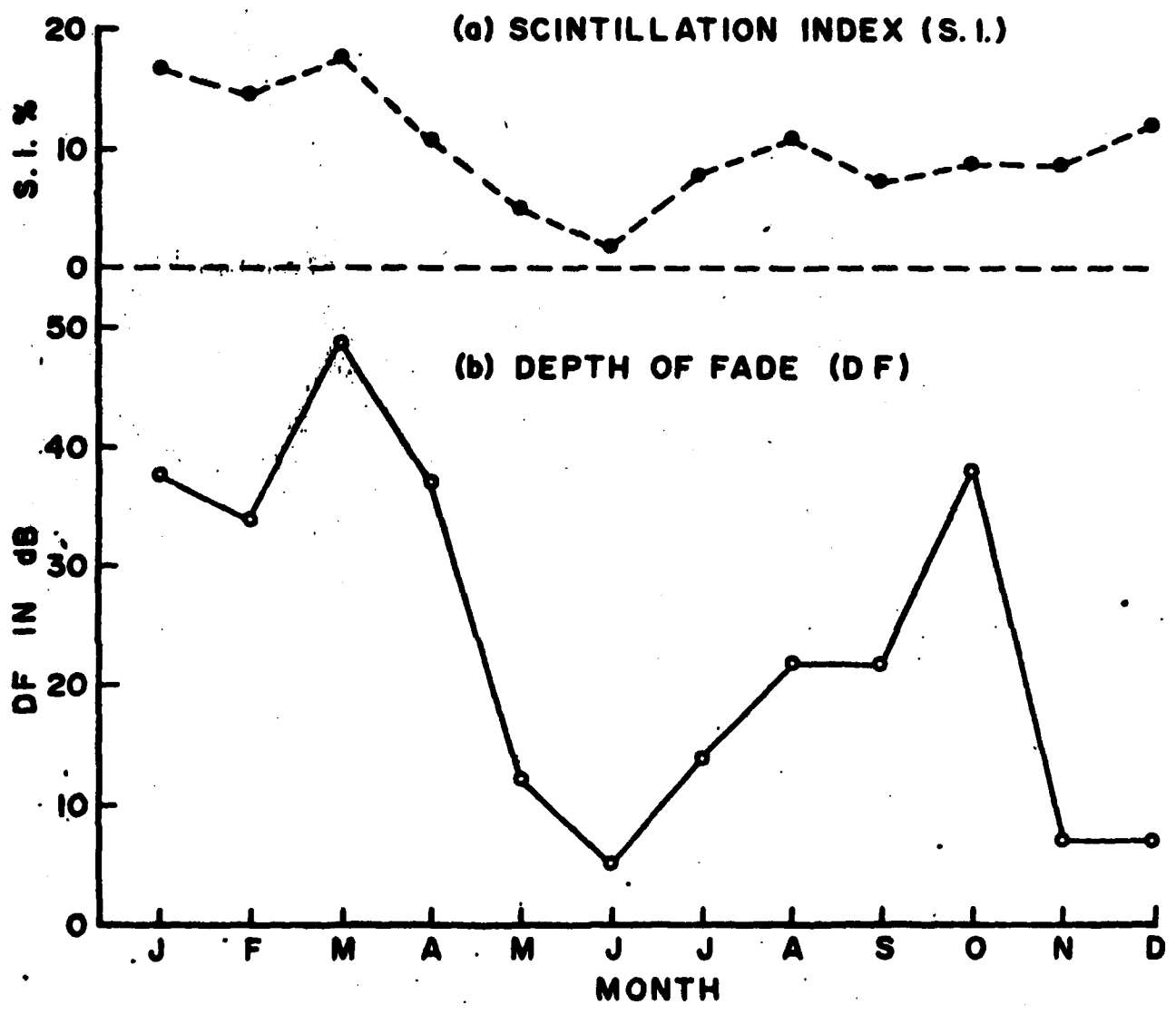


Figure 6

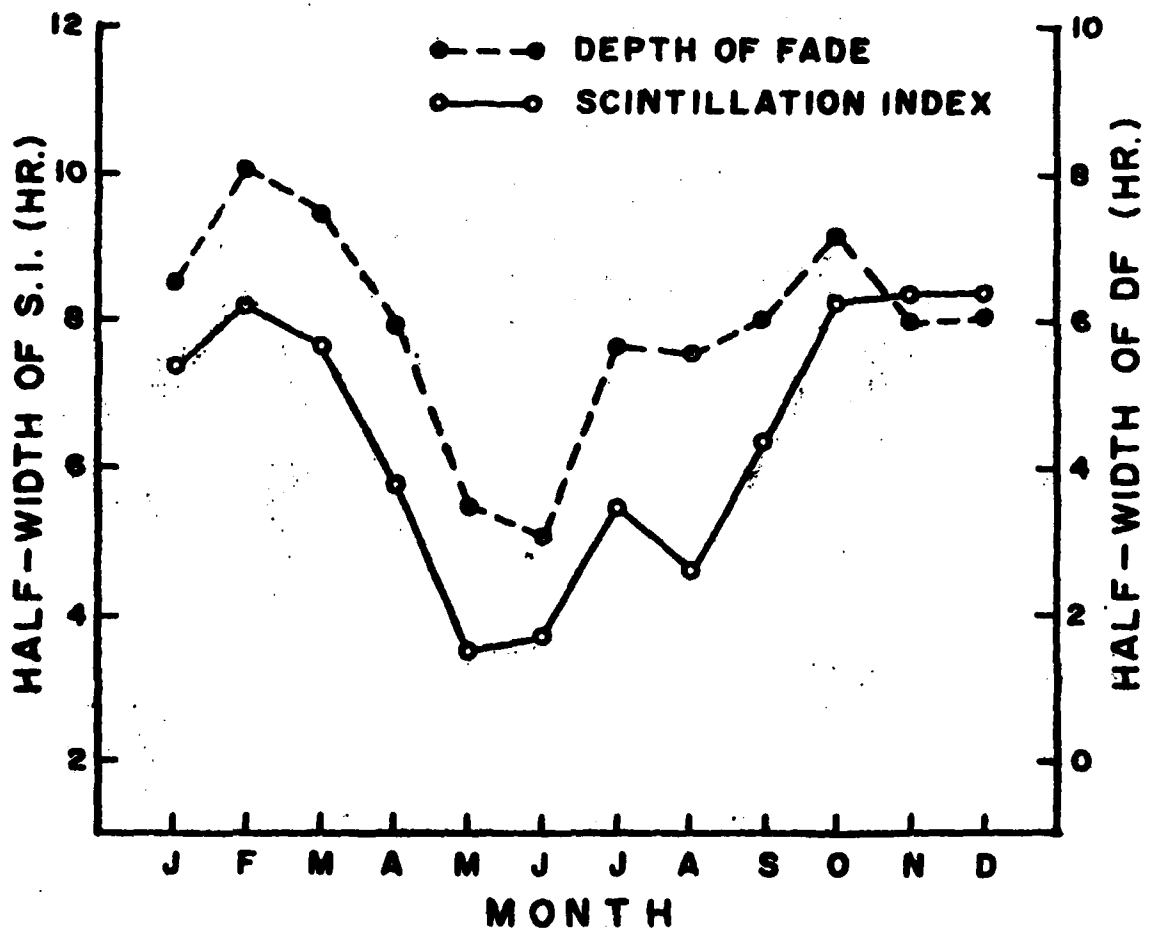


Figure 7

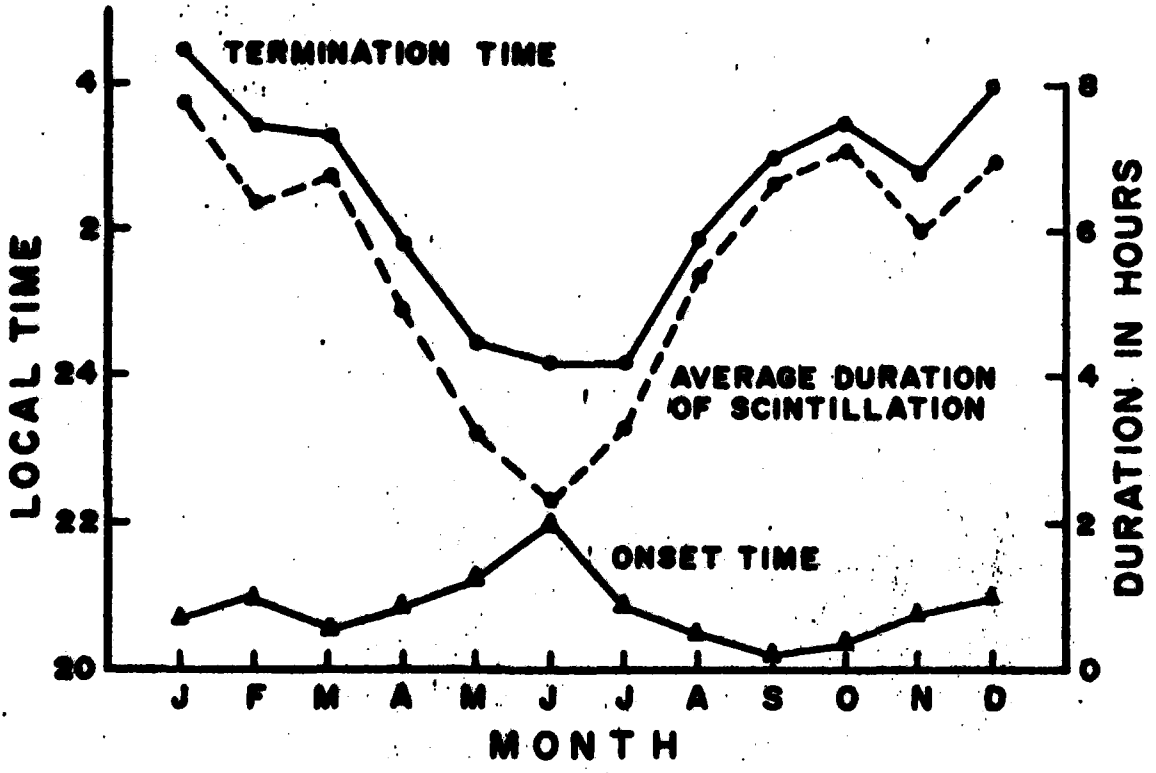


Figure 8

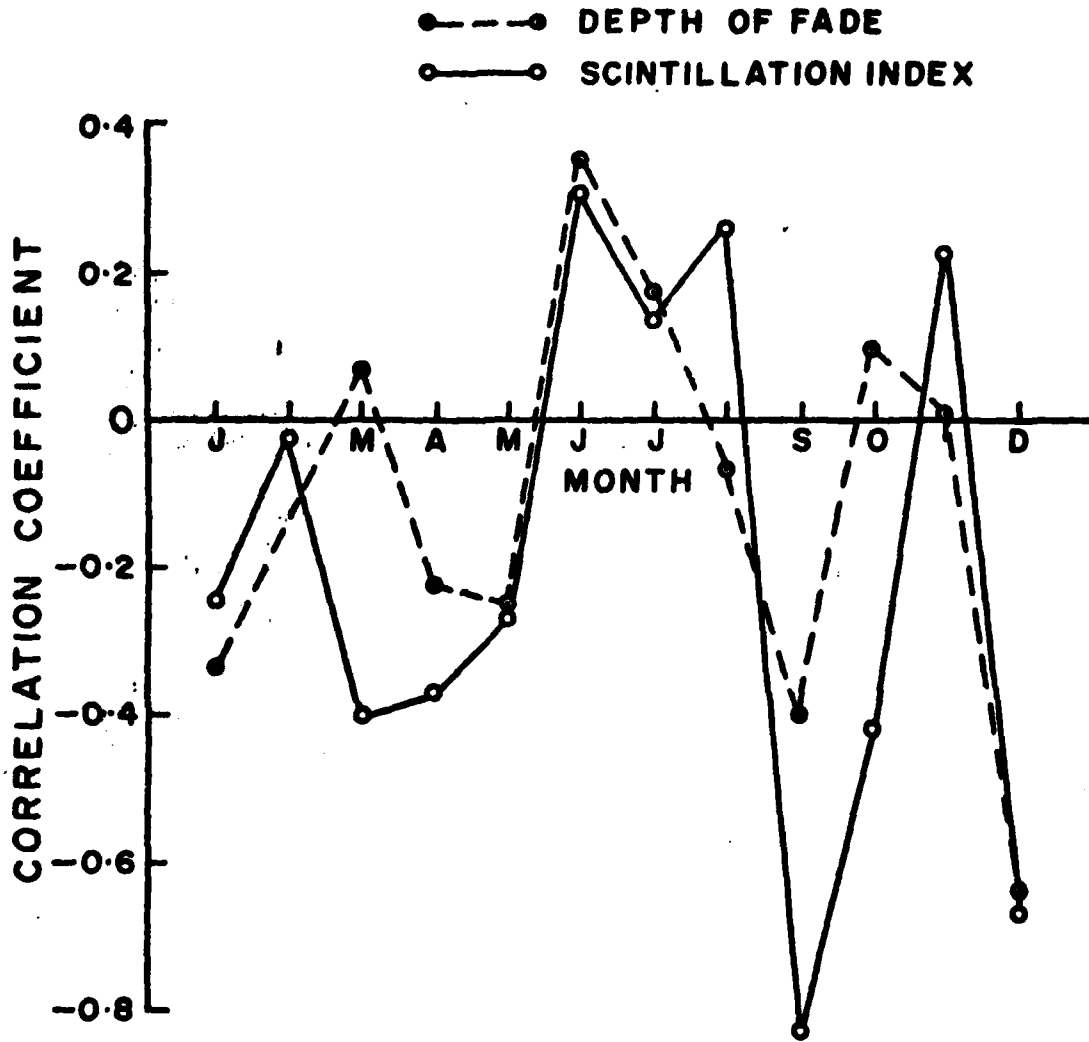


Figure 9